metals

MDPI

Article

Effect of Shielding Gas Volume Flow on the Consistency of Microstructure and Tensile Properties of 316L Manufactured by Selective Laser Melting

Ruochen Ding [1,2], Jun Yao [1,*], Baorui Du [1], Kailun Li [1], Tao Li [3], Lu Zhao [1,2] and Yumeng Guo [1,2]

[1] Institute of Engineering Thermophysics, Chinese Academy of Sciences, 11 Beisihuanxi Road, Beijing 100190, China; dingruochen@163.com (R.D.); dubaorui@iet.cn (B.D.); likailun@iet.cn (K.L.); zhaolu@iet.cn (L.Z.); guoyumeng@iet.cn (Y.G.)
[2] University of Chinese Academy of Sciences, Beijing 100049, China
[3] Sichuan Aerospace Zhongtian Power Equipment Co., Ltd., Chengdu 610100, China; litaoztdl@163.com
* Correspondence: yaojun@iet.cn

Abstract: In recent years, selective laser melting (SLM) has been widely used in aerospace, automobile, biomedicine and other fields. However, there still remain many challenges to obtain consistent parts at the different positions on the base plate, which could be harmful to the industrial mass-production. In SLM process, the process by-products that flow with the shielding gas may influence the microstructure and tensile properties of the parts placed on different positions of the base plate. In this study, the velocity field of the shielding gas with different shielding gas volume flows was simulated. The tensile properties of the samples fabricated with different shielding gas volume flow were experimentally studied. The results show that the shielding gas volume flow has a strong influence on the sample consistency, and proper increase in shielding gas volume flows can be beneficial to consistency and tensile strength.

Keywords: selective laser melting; shielding gas; tensile properties; microstructure

check for updates

Citation: Ding, R.; Yao, J.; Du, B.; Li, K.; Li, T.; Zhao, L.; Guo, Y. Effect of Shielding Gas Volume Flow on the Consistency of Microstructure and Tensile Properties of 316L Manufactured by Selective Laser Melting. *Metals* **2021**, *11*, 205. https://doi.org/10.3390/met11020205

Received: 5 January 2021
Accepted: 20 January 2021
Published: 22 January 2021

Publisher's Note: MDPI stays neutral with regard to jurisdictional claims in published maps and institutional affiliations.

Copyright: © 2021 by the authors. Licensee MDPI, Basel, Switzerland. This article is an open access article distributed under the terms and conditions of the Creative Commons Attribution (CC BY) license (https://creativecommons.org/licenses/by/4.0/).

1. Introduction

In recent years, additive manufacturing (AM) technology has been widely used in many fields, such as aerospace, automobile, biomedicine, etc. AM technology has the advantages of high material utilization, a shortened manufacturing period, lightweight structure and fabricate complex structures that traditional methods cannot process. SLM is one of the most widely used metal AM techniques, which has successfully processed various metal with excellent mechanical properties [1–4]. In the SLM manufacturing process, the high energy laser beam selectively melted the metal powder that has been deposited on the metal base plate with thin layers thickness of 15~100 μm [5,6]. The area of the laser beams selectively melted were based on the two-dimensional CAD data, and the two-dimensional CAD data were transferred from a three-dimensional model of the part. The metal powder was rapid melted and solidified under the selective scan of a high energy laser beam. When one layer is completely manufactured, the base platform lowers down by one-layer thickness and a new layer of metal powder is deposited on the powder bed. This process is repeated layer by layer, until all the parts are finished. The processing parameters of SLM have great influence on the microstructure and tensile properties of the fabricated parts [7,8], such as layer thickness, laser power, scan speed, hatch space, scan strategy, shielding gas, etc.

In general, the manufacturing environment of the SLM process must be protected by shielding gas. Therefore, the powder bed is set in a closed chamber, which is filled with shielding gas. The shielding gas is recirculated in a closed circuit with a filter. Because the shielding gas can prevent chemical reactions and limits the generation of process by-products in the working chamber, the shielding gas play a key role in the quality and consistency of

parts fabricated by SLM [9]. Furthermore, the shielding gas also play an important role in removing SLM process by-products such as spatter, welding fumes and condensate [10]. The by-products of the SLM process may cause laser attenuation and contaminate the powder. Therefore, much research has focused on the shielding gas in the SLM process.

Wang et al. [11] composed a blow-to-suction appliance as the model of the SLM working chamber to study the flow uniformity inside the working chamber, and the reliability of the simulation is verified by hot-wire velocity measurement and smoke flow visualization. The momentum exchange between the flow inlet and outlet have a great effect on the uniformity of the flow through the working chamber, and the uniformity of the flow increased with the increase of the outlet velocity of outlet area of the nozzle. Philo et al. [6] investigated the shielding gas flow and the by-product distribution in the SLM process by a multiphase computational fluid dynamics model. The experimental result of Hot Wire Anemometry was used to validated the multiphase computational fluid dynamics model. The results show that this model can accurately reflect the flow field in the working chamber.

Ferrar et al. [10] investigated the effect of inert gas flow on porosity and compression strength of a titanium lattice structure. The experimental results indicated that gas flow uniformity can seriously influence the compression strength and density of titanium lattice structures. Optimized gas flow can decrease porosity and improve the compression strength of the samples. Anwar et al. [12,13] experimentally studied the influence of inert shielding gas flow velocity on the mechanical property of SLM-fabricated AlSi10Mg. The result shows that the flow velocity has a great impact on the mechanical property of SLM fabricated AlSi10Mg than part placement. Moreover, when the laser scanning direction is against the gas flow, it can achieve better part quality. The researchers suggest that modification to optimize gas flow can improve part quality.

Bidare [14] combined high-speed imaging, schlieren imaging, and multi-physics modelling to investigate the influence of the interaction between the high energy laser beam and the metal powder. The results indicated that the shielding gas and the laser plume play a key role in the process of the heat, mass and momentum transfer. Uniform flow field plays an important role in reducing plume and particle pollution. Higher flow rate is beneficial to provide enough momentum to reduce the contamination of powder bed by by-products. Shen [15] investigated the Hastelloy X samples built by SLM with different gas flow velocities. The results show that when the shielding gas flow velocity is low, a greater lack of fusion defects can be found in the samples. The particle pickup velocity was also experimentally investigated to obtain the limit of further increasing the shielding gas flow velocity without influencing the powder bed. The relationship of porosity and particle pickup velocity was proposed as the reference of setting the lower and upper limits of shielding gas flow velocity in the SLM process.

The previous studies have shown that the shielding gas has a great influence on the SLM process. The by-products of the SLM process can be reduced by controlling shielding gas. The previous work on shielding gas was mainly focused on the characters of gas flow in the SLM machine's working chamber. These researches have proved that the flow field can significantly influence the properties of parts manufactured by SLM, but little attention has been focused on the relationship between gas flow and the consistency of tensile properties of parts at the different position on the base plate. Gas flow could influence the distribution of processing by-products, which may further affect the microstructure and tensile properties of the parts at different positions. It is very important to obtain a good repeatability in industrial mass-production. Therefore, the research into property uniformity of the parts manufactured by SLM is absolutely necessary.

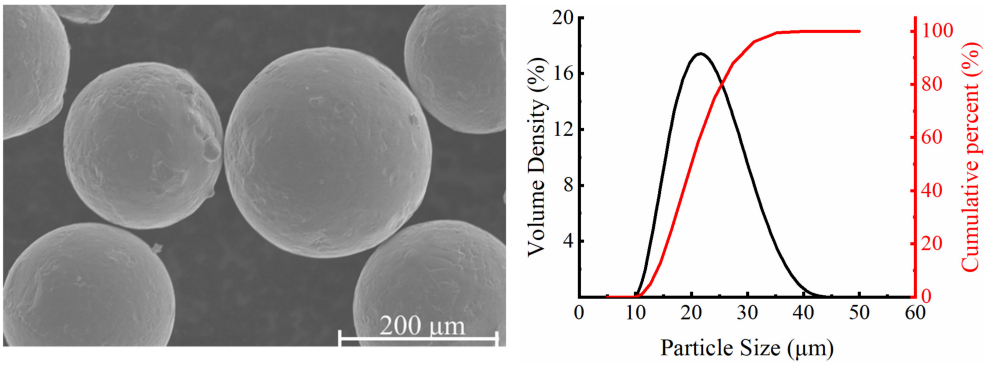
In summary, although the shielding gas has had a great impact on the SLM process, its influence on the consistency of the fabricated parts was rarely investigated. In this study, we aim to establish the relationship between the shielding gas volume flow and the consistency of the SLMed 316L parts in terms of microstructure and tensile properties. The velocity field of the shielding gas flow was simulated and the tensile properties of the 316L samples fabricated by SLM with different shielding gas volume flow were experimentally

researched. The purpose of this paper is to study the influence of the shielding gas volume flow on microstructure and tensile properties of the 316L samples at different positions in the base plate and obtain consistent microstructure and tensile properties at different positions of the base plate via shielding gas volume flow control.

2. Materials and Methods

2.1. Material

The samples for microstructure and tensile properties test were made from 316L by SLM. The metal powder used in this study was gas atomized 316L stainless steel powder, which was produced by LPW Technology Ltd., Widnes, UK. The 316L stainless steel powder sample was analysed by FEI Inspect F50 Scanning Electron Microscope (SEM, FEI, Hillsboro, OR, USA). The surface morphology of the 316L stainless steel powder is provided in Figure 1a, the spherical particles with a smooth surface are conducive to the SLM process and the production of dense 316L stainless steel samples. Figure 1b shows the particle size distribution of the 316L stainless steel powder. It can be seen that the particle size distribution of the powder is 10~45 μm. To control the variables, the virgin powder was used for every set of the samples, the oxygen content of the virgin powder is 0.05%.



(**a**) The surface morphology of the 316L stainless steel powder

(**b**) The particle size distribution of the 316L stainless steel powder

Figure 1. The surface morphology and particle size distribution of the 316L stainless steel powder.

2.2. Numerical Modelling

In the Eulerian–Lagrange model, Computational Fluid Dynamics (CFD), is used for the gas flow, which involves the conservation of mass and momentum. In this study, because the shielding gas flow has a relatively slow velocity, the Reynolds number of the fluid phase was low as well. Therefore, a k- turbulence model can better predict the flow in a confined space. Turbulent kinetic energy transport equation:

$$\frac{\partial(\rho k)}{\partial t} + \frac{\partial(\rho k u_i)}{\partial x_i} = \frac{\partial p}{\partial x_j}\left[\left(\mu + \frac{\mu_t}{\sigma_k}\right)\frac{\partial k}{\partial x_j}\right] + G_k + G_b - \rho\varepsilon - Y_M + S_k \quad (1)$$

Energy dissipation transport equation:

$$\frac{\partial(\rho\varepsilon)}{\partial t} + \frac{\partial(\rho\varepsilon u_i)}{\partial x_i} = \frac{\partial p}{\partial x_j}\left[\left(\mu + \frac{\mu_t}{\sigma_\varepsilon}\right)\frac{\partial \varepsilon}{\partial x_j}\right] + \rho C_1 S\varepsilon - \rho C_2 \frac{\varepsilon^2}{k + \sqrt{\nu\varepsilon}} + C_{1\varepsilon}\frac{\varepsilon}{k}C_{3\varepsilon}G_b + S_\varepsilon \quad (2)$$

where, G_k is the turbulence kinetic energy generated by the mean velocity gradients; G_b is the turbulence kinetic generated by buoyancy; $C_{1\varepsilon}$, C_2, and $C_{3\varepsilon}$ are constants; σ_k is the turbulent Prandtl numbers for k; σ_ε are the turbulent Prandtl numbers for ε; Y_m is the influence of the fluctuating dilatation in compressible turbulence on the overall dissipation rate; ϱ is the argon density; u_i is the gas velocity and x_i is the position vector; t is the time step; μ is the molecular viscosity of the fluid; μ_t is the turbulent viscosity; and S_k and S_ε are user-defined source terms.

The geometry of the shielding gas flow volume and the mesh of the volume is shown in Figure 2. The structured quadrilateral meshes was created using the ICEM (ANSYS, Inc., Canonsburg, PA, USA). The structured quadrilateral meshes is preferable for CFD simulations, and the grid independence was verified. The mass flow inlet boundary condition is defined as a mass flow inlet boundary at the beginning of the inlet. The shielding gas volume flow was set at 500 L/min, 550 L/min and 600 L/min of each set in the experiments. The shielding gas flow velocity was calculated from the gas volume flow as 4.94 m/s, 5.48 m/s and 5.95 m/s. The outlet boundary condition was defined as an outflow boundary condition.

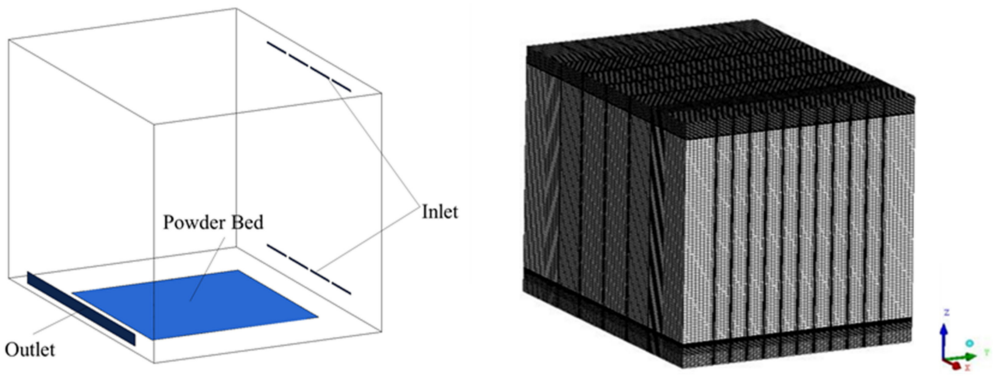


Figure 2. The geometry of the shielding gas flow volume and the mesh of the volume.

2.3. Sample Model

In order to investigate the effect of gas flow on the consistency of microstructure and tensile properties of 316L fabricate by SLM, a number of sets of samples was fabricated as shown in Figure 3. The dimensions of the base plate are 300 mm in X and Y direction. The overall size of each uniaxial tensile samples is 90 × 15 × 4 mm (length × width × height) and microscopic samples is 10 × 10 × 10 mm (length × width × height), designed with each sample being individually identified. The uniaxial tensile samples of each set were built on the base plate in a 3 × 4 array (5 mm and 85 mm spacing in X and Y directions). For each set, the samples used for microscopic characterization were built on the base plate in 4 arrays (85 mm spacing in Y direction).

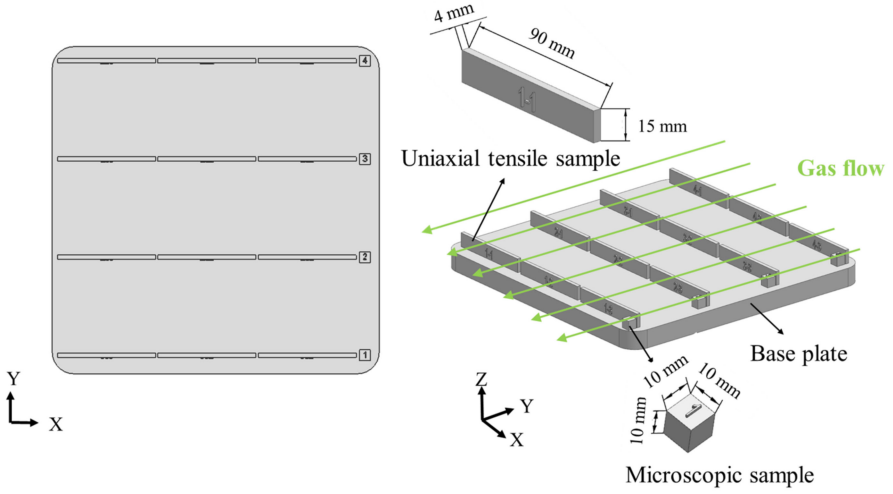
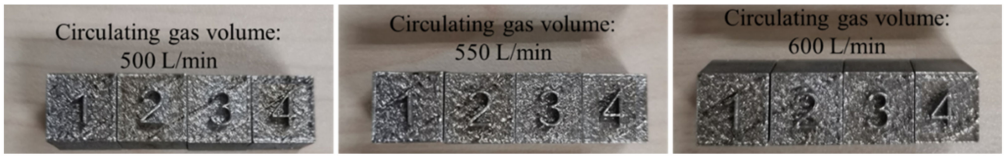


Figure 3. The CAD model of the test samples.

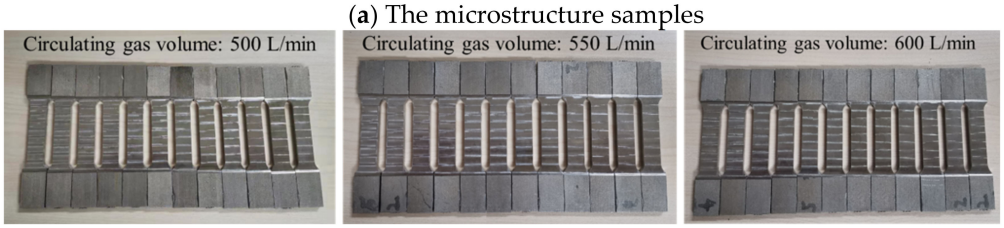
2.4. Manufacturing Parameters

The SLM machine used in this study was a LASERTEC 30 SLM printer (DMG, Bielefeld, Germany) from DMG. The laser power used to fabricate the samples was 254 W, the layer thickness of the powder was 50 μm, laser scanning speed was 1000 mm/s and scan

strategy of 67° interlayer rotation scan. Argon serves as a shielding gas to protect metals from oxidation during melting, the purity of argon is equal or greater than 99.999%, the shielding gas volume flow was 500 L/min, 550 L/min and 600 L/min for each set. The base plate was preheated to 100 °C to reduce the thermal stress during manufacturing. Before manufacturing begins, argon is filled into the working chamber as a shielding gas, and the process begins when the oxygen content of the working chamber is below 0.2%. Wire-electrode cutting was applied to separate the printed samples from the base plate. The microstructure test samples are displayed in Figure 4a and the uniaxial tensile samples machined by 5-axises Machining Centre are displayed in Figure 4b.



(**a**) The microstructure samples

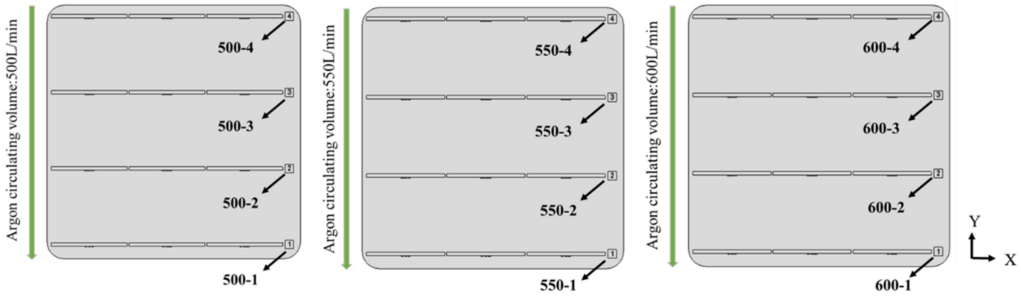


(**b**) The uniaxial tensile samples

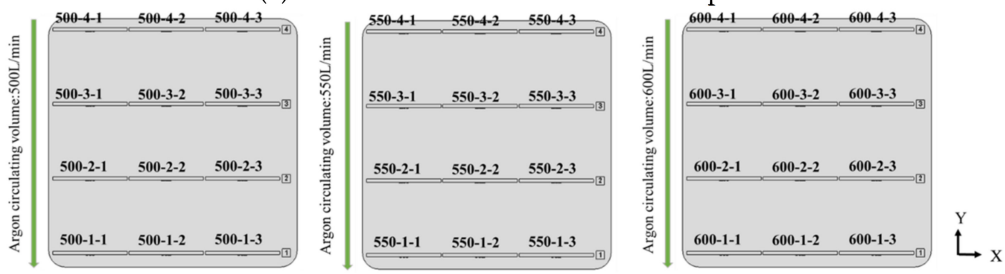
Figure 4. The samples fabricated by SLM with different shielding gas volume flow.

2.5. Material Characterization and Mechanical Test

The sample number of microstructure and uniaxial tensile samples were shown in Figure 5. The microstructure test samples were hot-mounted and polished. The microstructure and metallographic of the samples were observed by SEM and the optical microscope (FEI, Hillsboro, OR, USA), respectively. An Instron 5567 testing machine (Instron, Norwood, MA, USA) was used to test the uniaxial tensile properties of the samples at room temperature under uniaxial loading based on ISO 6892-1:2019 standard [16]. The original gauge length is marked on the samples before testing.



(**a**) The number of microstructure samples



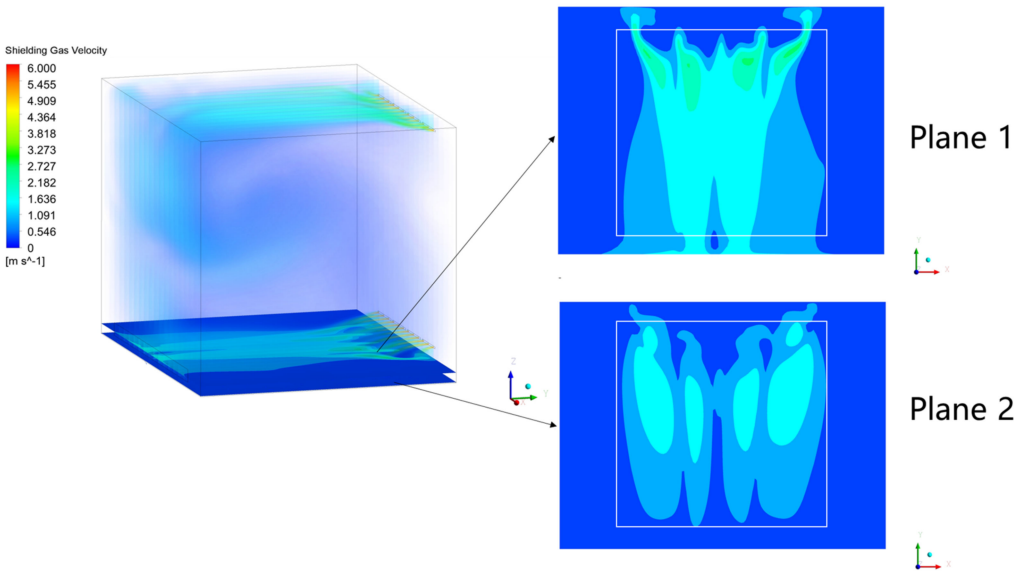
(**b**) The number of uniaxial tensile samples

Figure 5. The number of the samples.

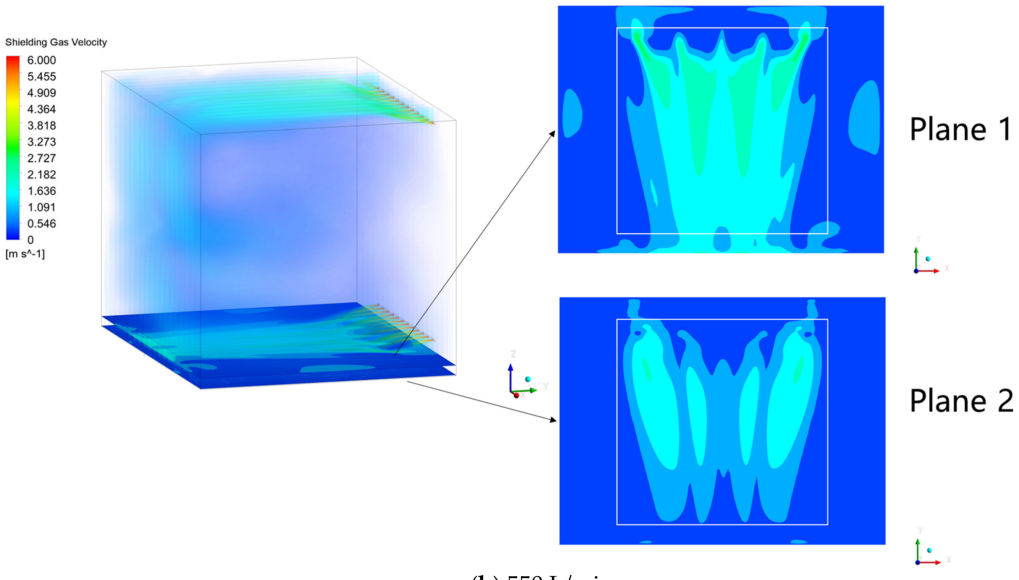
3. Results

3.1. Velocity Fields in the Working Chamber

The velocity fields in the working chamber with different shielding gas volume flows was analyzed by fluent. The velocity field of the working chamber under different shielding gas volume flows is shown in Figure 6. The distance of Plane 1 and Plane 2 from the base plate is 15 mm and 1 mm respectively, and the velocity distributions on Plane 1 and Plane 2 were derived for more details. The results indicated that with the increase of shielding gas volume flow, the area of high-velocity ($\geq$1 m/s) shielding gas on Plane 1 and Plane 2 become larger, high-velocity shielding gas can effectively clean the by-products and reduce the pollution of by-products to the powder bed. The velocity of shielding gas is higher in the middle position above the substrate and lower near the shielding gas inlet. When the shielding gas volume flow is 500 L/min, there is a large area of low-velocity shielding gas above the powder bed. With the shielding gas volume flow increase to 550 L/min and 600 L/min, most areas of the powder bed can be covered by a high-velocity shielding gas.

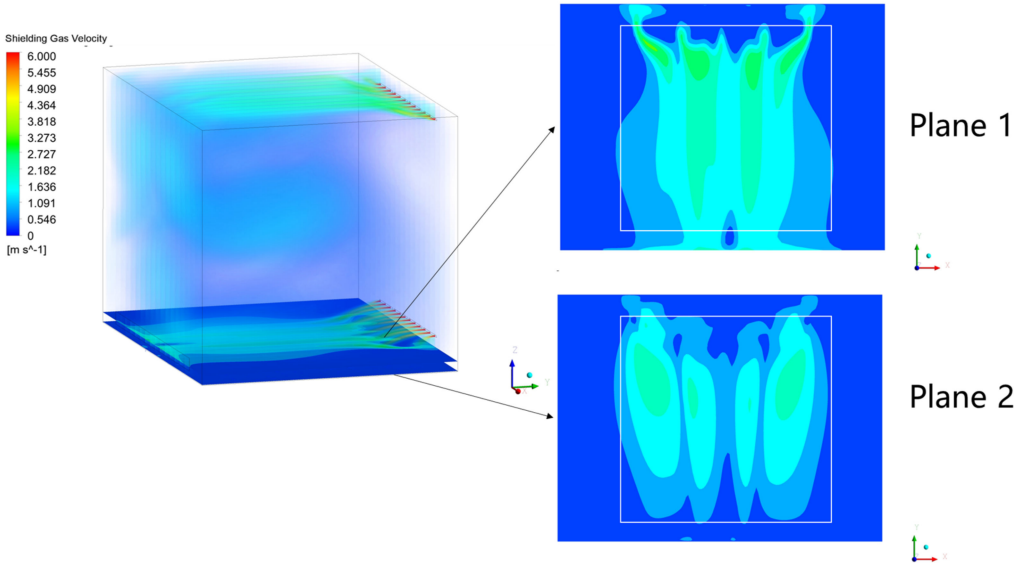


(**a**) 500 L/min



(**b**) 550 L/min

Figure 6. *Cont.*



(**c**) 600 L/min

Figure 6. The velocity fields in the working chamber with different shielding gas volume flows.

3.2. Microstructures

The microstructure images of the samples fabricated by SLM with different shielding gas volume flows are shown in Figure 7. Under the condition of 500 L/min, many particle inclusions along with the lack of fusion defects can be observed in the samples. When the shielding gas volume flow was 550 L/min or 600 L/min, no lack of fusion defects was observed, only a few small pores and inclusion defects inside the samples.

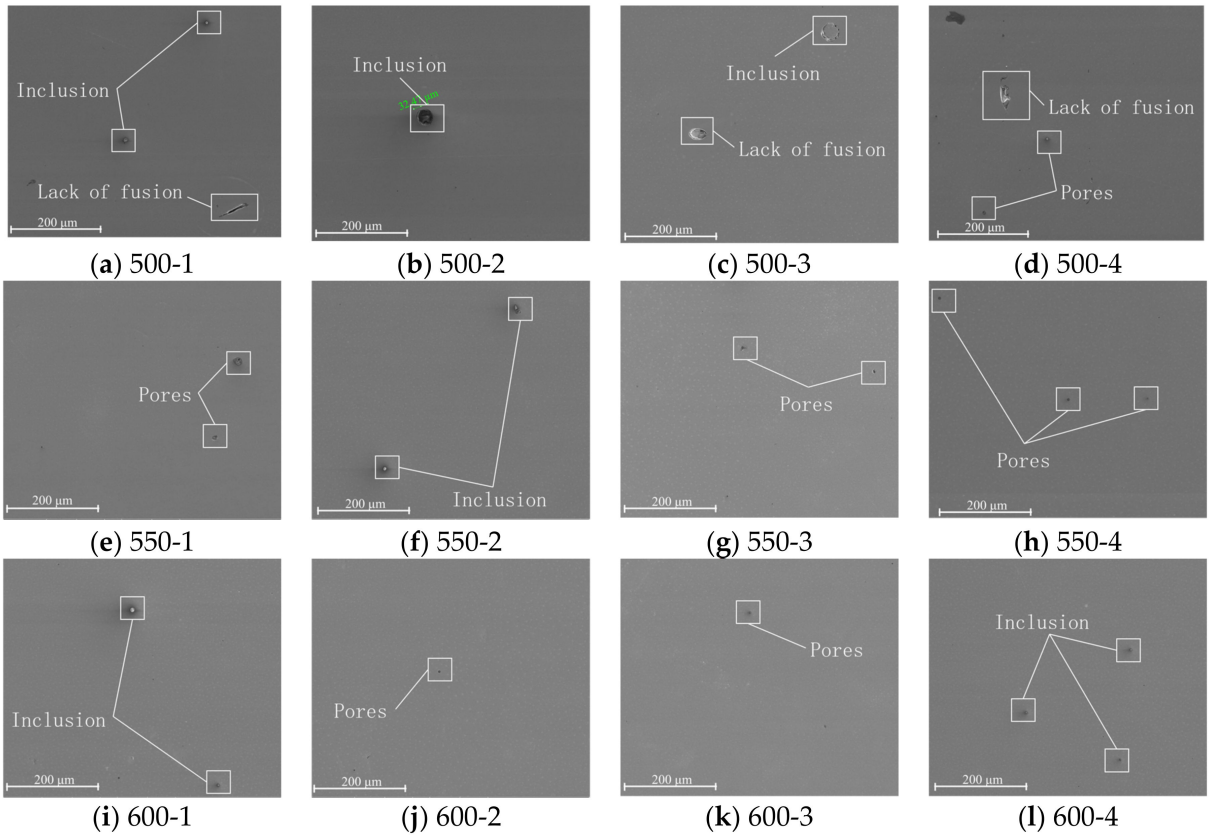


Figure 7. The microstructures of 316L sample fabricated with different shielding gas volume flows.

3.3. Metallographic

Figure 8 shows the metallographic diagram of samples at different positions on the substrate under different shielding gas volume flows. In the manufacturing process, the metal powder under the action of high energy laser rapid melting and solidification. Each layer of the samples is composed of a multiple overlapped scan line, therefore, there is a great difference in metallographic structure between selected laser melted parts and traditional casting parts. Obvious trace of sintering line can be observed from the metallographic microstructure of the cross section of the sample. The overlaps between sintering lines have good quality and the sintering lines are 67° intersected. As can be seen from the figure, with the increase in the protective gas flow, there was no significant difference in the metallographic structure of the samples. Although shielding gas volume flow has an obvious influence on defects in the samples, the samples fabricate with different shielding gas volume flows have no obvious difference on the metallographic.

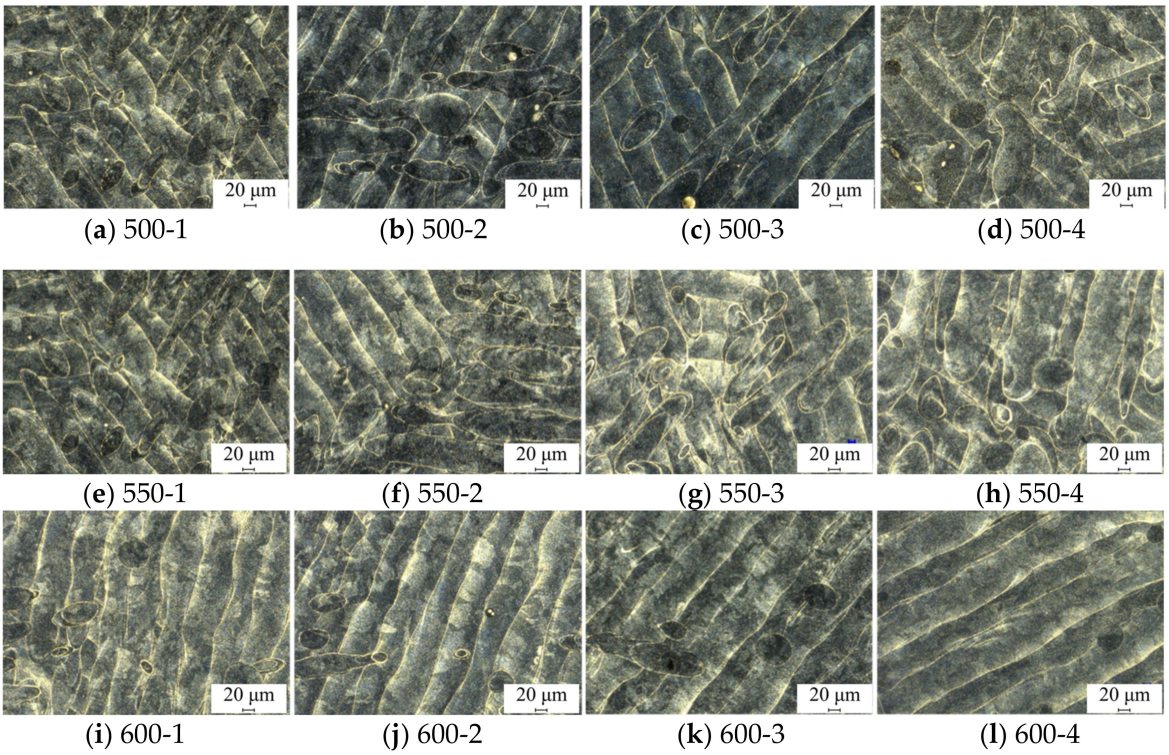


Figure 8. The metallographic of 316L samples fabricated with different shielding gas volume flows.

3.4. Tensile Properties

The uniaxial tensile test stress-strain curves of 316L sample fabricated by SLM under different shielding gas volume flows are illustrated in Figure 9. Every curve is the average of the uniaxial tensile samples at the same Y position. There are significant differences among the tensile properties of samples at different positions when the shielding gas volume flow was 500 L/min. The tensile strength of 500-1 and 500-2 samples are much higher than that of the 500-4 sample. When the shielding gas volume flow was 550 L/min and 600 L/min, there is no significant differences among the tensile properties of samples at different positions. With the increase in shielding gas volume flows, the difference in the tensile properties of the samples at different positions on the base plate gradually narrowed.

The Young's Modulus (E) is obtained by calculating the slope of the stress-strain curve in the linearity stage. The yield strength (R_s) and tensile strength (R_m) of the samples can be directly obtained from the uniaxial tensile test stress-strain curves. The elongation of the samples was observed by the original gauge length and final gauge length after fracture. Figure 10 shows the average Young's Modulus, yield strength, tensile strength and elongation

of each set with error bars. The Young's Modulus of the samples increases with the increases of the shielding gas volume flow, but there is no significant difference of the variance change with the increases in the shielding gas volume flow. The average yield strength and tensile strength of the samples increases with the increases of the shielding gas volume flow, and the variance decreases with the increases in the shielding gas volume flow. The average elongation (η) of the samples decreases with the increases in the shielding gas volume flow, and the variance decreases with the increases in the shielding gas volume flow.

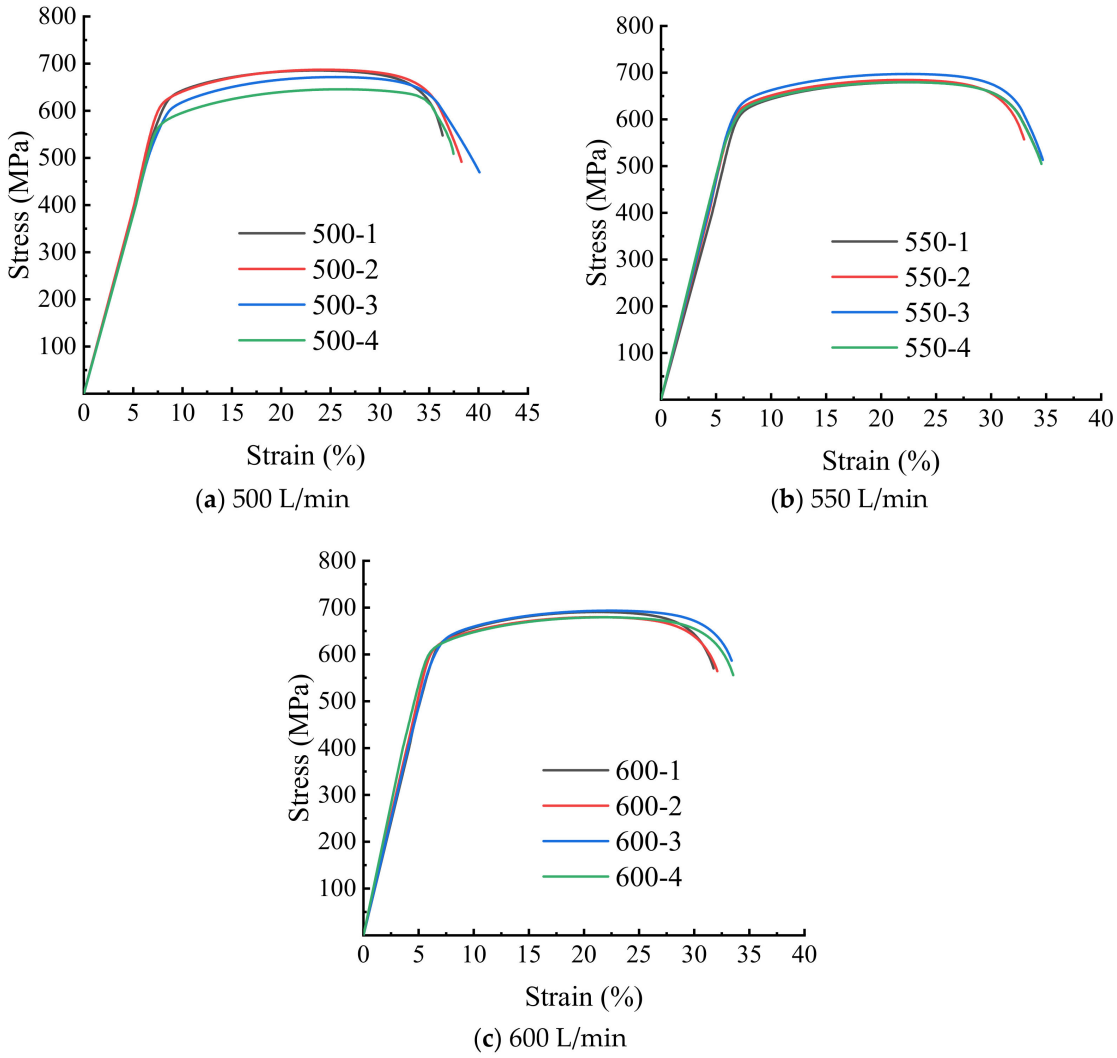


Figure 9. The uniaxial tensile test stress-strain curves of 316L sample fabricated with different shielding gas volume flows.

3.5. Fracture Analysis

Figure 10 shows the fracture surfaces of the samples fabricated by SLM under different shielding gas volume flows. The fracture surfaces of the samples are completely covered with fine dimples, indicating an excellent energy absorbing ability and obvious plastic fracture characteristics, which shows that the 316L manufactured by SLM has excellent tensile strength and a high elongation rate. Figure 11a clearly reveals the defects in morphologies, i.e., pores, incomplete fusion defects and inclusions. More holes can be observed in the fracture surfaces of 500-3-2. Moreover, compared to the typical ductile fracture of 500-3-2, some brittle-like fracture characteristics are displayed in the fracture surfaces of 550-3-2 and 600-3-2 samples (as seen in Figure 11b,c).

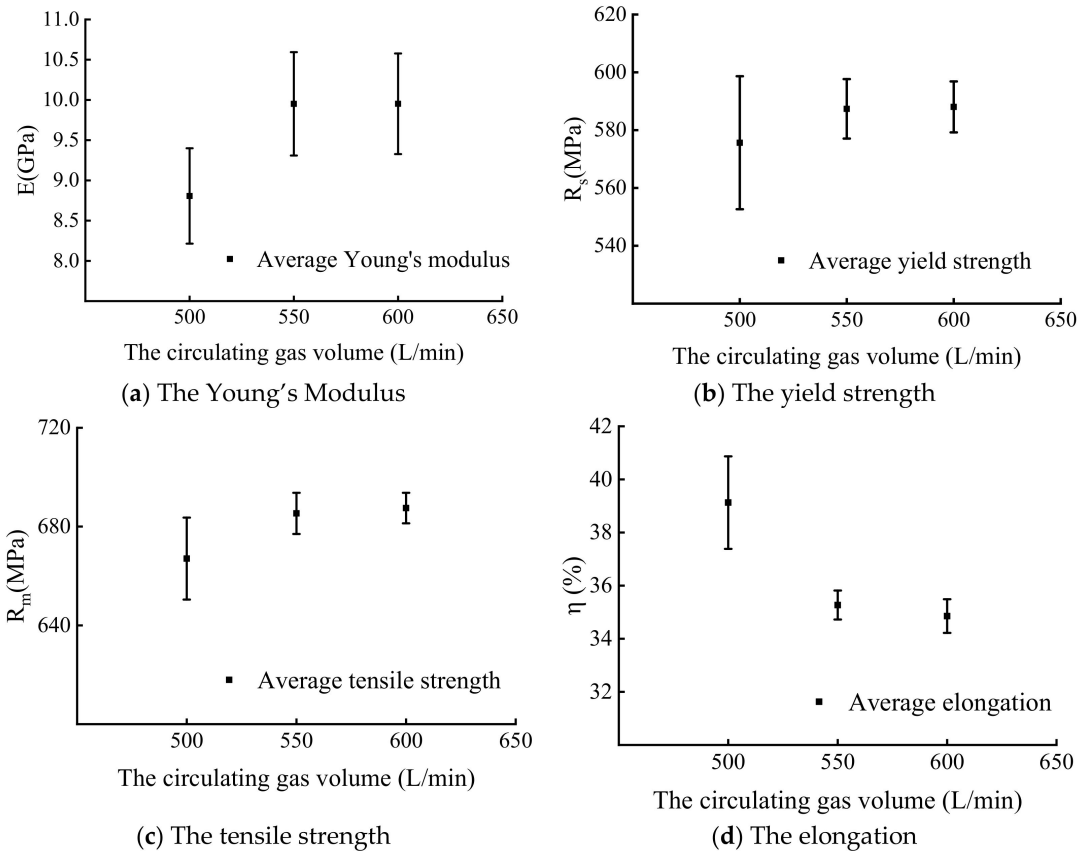


Figure 10. The average elongation and tensile strength with error bars of each set.

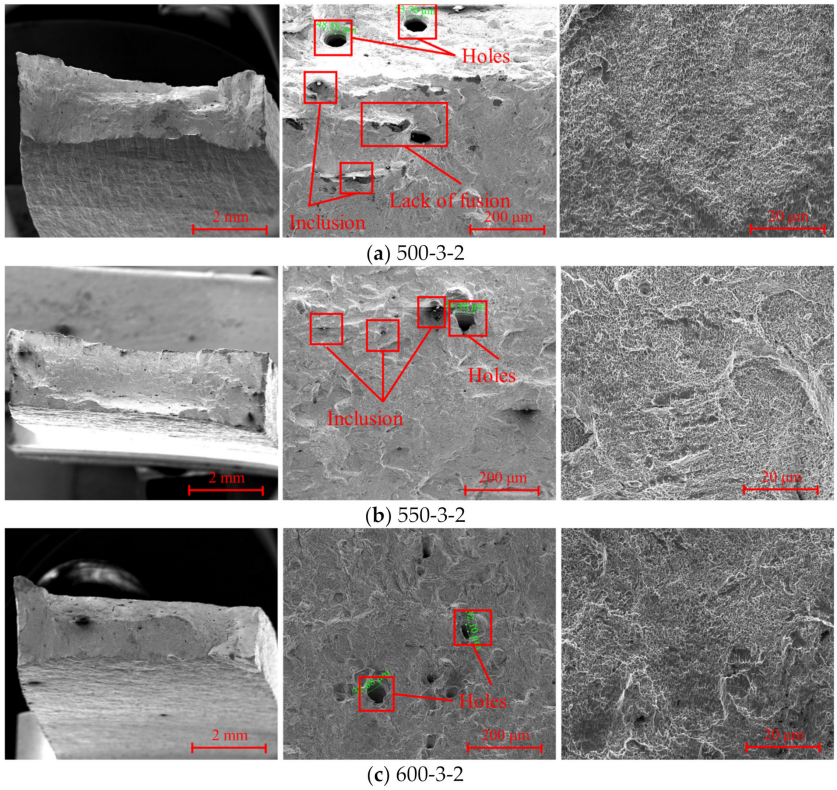


Figure 11. Fractography of the SLM in the uniaxial tensile samples fabricated under different shielding gas volume flows after tensile tests.

4. Discussion

Generally, there are three kinds of defects inside the samples fabricated by SLM: pores, lack of fusion and inclusion. The defects-forming mechanism in the SLM process are shown in Figure 12. The internal pores are mainly caused by hollow powder particles and the shielding gas in the SLM working chamber. The gas was wrapped into the molten pool and trapped in the solidified part. The lack of fusion defects has typical features of a large size, an irregular shape and un-melted metal powder inclusions. The reason for the lack of fusion defects is that the laser energy is not sufficient enough to melt the whole metal powder. The inclusion defect was characterized by an irregular and elliptical shape with inclusions filling in the hollow. The inclusion defect was mainly caused by the refractory by-product mixing with the metal powder, making it difficult to melt during the process of the next layer included in the sample.

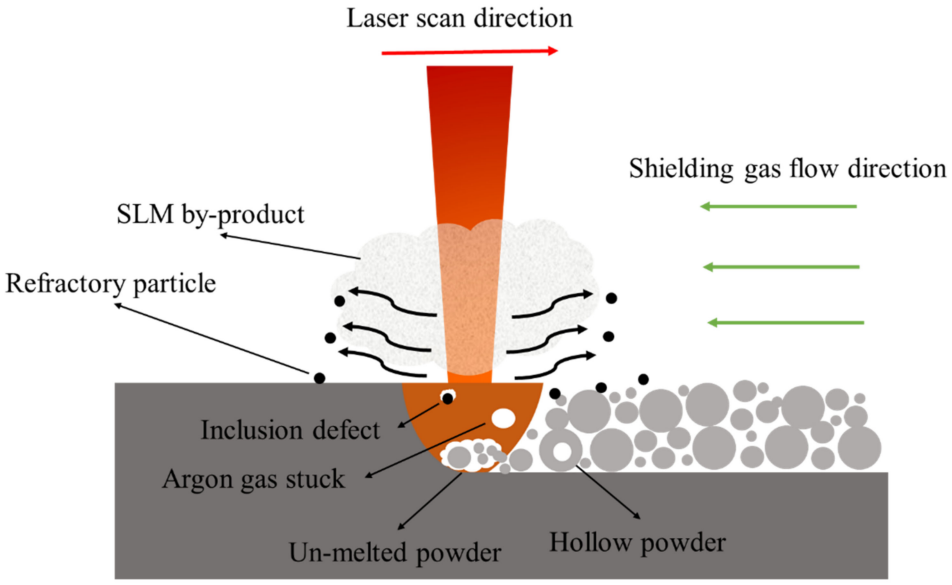


Figure 12. The defects forming the mechanism in the SLM process.

The cleaning efficiency of shielding gas to SLM by-products is directly determined by the flow velocity of shielding gas. Under the premise of not exceeding the pickup velocity, the higher the flow velocity, the better the cleaning effect. When the shielding gas volume flow was 500 L/min, there was a large area of low-velocity shielding gas area above the powder bed. In the low-velocity area, the SLM by-product cannot be cleaned in time, which caused laser attenuation and the powder bed contamination. From the shielding gas velocity simulation, the low-velocity areas are near the gas inlet. The microstructural observation agreed with the simulation results, and more defects were observed in the samples placed at the position near to the gas inlet, which indicates that the sample quality in the low-velocity area is poor. Because of the laser plume attenuation, the laser energy is not sufficient enough to melt the powder [15], which would cause a lack of fusion defects inside the samples. The powder bed contamination could cause more inclusion defects. As a result, the tensile strength of the sample near the gas inlet (500-4) is the lowest.

The tensile test results of the samples show that the tensile strength of the samples increases with the increase in the shielding gas volume flow, because the working chamber has a better process condition when the SLM process has a higher shielding gas volume flow. With the increase in the shielding gas volume flow, the high-velocity area covers the whole powder bed, which can lead to a lower laser beam attenuation and less pollution on the powder bed, and the defects inside the samples have significantly reduced. A better process condition improved the strength and consistency of the samples. The fracture surfaces of 500-3-2 clearly reveals a large amount of defects, which may cause stress concentration and become the crack initiation points. The crack would further propagate

along the defects until the sample fractured. These defects were responsible for the poor strength of the sample fabricate, with a 500 L/min shielding gas volume flow.

5. Conclusions

In this paper, the shielding gas flow was simulated, the microstructure and tensile properties of the samples fabricated with different shielding gas volume flows were experimental studied. The main findings of the study are summarized as follows:

- With the increase in the shielding gas volume flow, the area of high-velocity shielding gas above the base plate increased accordingly. When the shielding gas volume flow was 500 L/min, there was a large area of low-velocity shielding gas area above the powder bed, especially near the gas inlet and outlet. With the shielding gas volume flow increased to 550 L/min and 600 L/min, most areas of the powder bed could be covered by a high-velocity shielding gas.
- Under the shielding gas volume flow at 500 L/min, samples placed in a position near the gas inlet had more defects than the samples placed in the middle position of the base plate. When the shielding gas volume flow was 550 L/min and 600 L/min, only a few defects were found inside the samples. The defects inside the samples decreased with the increase in the shielding gas volume flow.
- The difference in tensile properties of the samples at different positions on the base plate gradually narrowed with the increase in shielding gas volume flow. The Young's Modulus of the samples increased with the increases in the shielding gas volume flow, but there was no significant difference in the variance change with the increases in the shielding gas volume flow. The yield strength and tensile strength of the samples increased with the increase in the shielding gas volume flow, and the elongation decreased with the increase in the shielding gas volume flow. When the shielding gas volume flow was 500 L/min, the samples with the high tensile strength were placed on the middle and bottom positions of the substrate. When the shielding gas volume flow was 550 L/min and 600 L/min, the samples with high strength could be obtained at most positions in the substrate.

Author Contributions: Conceptualization, R.D. and J.Y.; data curation, L.Z.; formal analysis, Y.G.; funding acquisition, B.D.; investigation, R.D.; methodology, T.L.; supervision, J.Y.; writing—original draft, R.D.; writing—review and editing, K.L. All authors have read and agreed to the published version of the manuscript.

Funding: This work was supported by the National Science and Technology Leading Talents Project (Y71Z01BBA1).

Institutional Review Board Statement: Not applicable.

Informed Consent Statement: Not applicable.

Data Availability Statement: All data generated or analysed during this study are included in this article.

Conflicts of Interest: The authors declare no conflict of interest.

References

1. ASTM. *ISO/ASTM 52900:2015(E), Standard Terminology for Additive Manufacturing—General Principles—Terminology*; International Organization for Standardization: Geneva, Switzerland, 2015.
2. Moussaoui, K.; Rubio, W.; Mousseigne, M.; Sultan, T.; Rezai, F. Effects of Selective Laser Melting additive manufacturing parameters of Inconel 718 on porosity, microstructure and mechanical properties. *Mater. Sci. Eng.* **2018**, *735*, 182–190. [CrossRef]
3. Wei, P.; Wei, Z.; Chen, Z.; Du, J.; He, Y.; Li, J.; Zhou, Y. The AlSi10Mg samples produced by selective laser melting: Single track, densification, microstructure and mechanical behavior. *Appl. Surf. Sci.* **2017**, *408*, 38–50. [CrossRef]
4. Stef, J.; Poulon-Quintin, A.; Redjaimia, A.; Ghanbaja, J.; Ferry, O.; De Sousa, M.; Gouné, M. Mechanism of porosity formation and influence on mechanical properties in selective laser melting of Ti-6Al-4V parts. *Mater. Des.* **2018**, *156*, 480–493. [CrossRef]
5. Suryawanshi, J.; Prashanth, K.; Ramamurty, U. Mechanical behavior of selective laser melted 316L stainless steel. *Mater. Sci. Eng. A* **2017**, *696*, 113–121. [CrossRef]

6. Philo, A.M.; Butcher, D.; Sillars, S.; Sutcliffe, C.J.; Sienz, J.; Brown, S.G.R.; Lavery, N.P. A Multiphase CFD Model for the Prediction of Particulate Accumulation in a Laser Powder Bed Fusion Process. *CFD Modeling Simul. Mater. Process.* **2018**, 65–76. [CrossRef]
7. Donik, Č.; Kraner, J.; Paulin, I.; Godec, M. Influence of the Energy Density for Selective Laser Melting on the Microstructure and Mechanical Properties of Stainless Steel. *Metals* **2020**, *10*, 919. [CrossRef]
8. Chen, W.; Yin, G.; Feng, Z.; Liao, X. Effect of Powder Feedstock on Microstructure and Mechanical Properties of the 316L Stainless Steel Fabricated by Selective Laser Melting. *Metals* **2018**, *8*, 729. [CrossRef]
9. Ladewig, A.; Schlick, G.; Fisser, M.; Schulze, V.; Glatzel, U. Influence of the shielding gas flow on the removal of process by-products in the selective laser melting process. *Addit. Manuf.* **2016**, *10*, 1–9. [CrossRef]
10. Ferrar, B.; Mullen, L.; Jones, E.; Stamp, R.; Sutcliffe, C.J. Gas flow effects on selective laser melting (SLM) manufacturing performance. *J. Mater. Process. Technol.* **2012**, *212*, 355–364. [CrossRef]
11. Wang, W.-C.; Chang, C.-Y. Flow analysis of the laminated manufacturing system with laser sintering of metal powder. Part I: Flow uniformity inside the working chamber. *Int. J. Adv. Manuf. Technol.* **2017**. [CrossRef]
12. Bin Anwar, A.; Ibrahim, I.H.; Pham, Q.-C. Spatter transport by inert gas flow in selective laser melting: A simulation study. *Powder Technol.* **2019**. [CrossRef]
13. Anwar, A.B.; Pham, Q.-C. Selective laser melting of AlSi10Mg: Effects of scan direction, part placement and inert gas flow velocity on tensile strength. *J. Mater. Process. Technol.* **2017**, *240*, 388–396. [CrossRef]
14. Bidare, P.; Bitharas, I.; Ward, R.M.; Attallah, M.; Moore, A. Fluid and particle dynamics in laser powder bed fusion. *Acta Mater.* **2018**, *142*, 107–120. [CrossRef]
15. Shen, H.; Rometsch, P.; Wu, X.; Huang, A. Influence of Gas Flow Speed on Laser Plume Attenuation and Powder Bed Particle Pickup in Laser Powder Bed Fusion. *JOM* **2020**, *72*, 1039–1051. [CrossRef]
16. *ISO 6892-1:2019(E), Metallic Materials—Tensile Testing—Part 1: Method of Test at Room Temperature*; International Organization for Standardization: Geneva, Switzerland, 2019.